Analytical Study of the Thermal Conductivity and Resistivity Properties of Zig-Zag Single-Walled (8,0) Carbon Nanotube Using Deng-Fan-Hulthen Potential Model

Otete, Ikechukwu[1], Abiodun, Isaac Chukwutem[2], AND Odezuligbo, Ikenna Emmanuel[3,*]

[1]*Department of Physics, Federal University, Otuoke, P.M.B 126, Bayelsa State Nigeria*

[2]*Department of Physics, Federal University, Otuoke, P.M.B 126, Bayelsa State Nigeria*

[3]*Department of Physics, Creighton University, Omaha, Nebraska 68131, U.S.A*

∗Ikennaodezuligbo@creighton.edu

Abstract

This study provides a detailed analysis of the thermal conductivity and resistivity of a zig-zag single-walled (8,0) carbon nanotube using the Deng-Fan-Hulthen potential model. By employing the Nikiforov-Uvarov method to solve the Schrödinger equation, we derive expressions for the energy eigenvalues and eigenfunctions under magnetic and Aharonov-Bohm (AB) flux fields. The partition function was calculated, and the thermal conductivity and resistivity properties were evaluated. Results indicate that magnetic and AB flux fields exponentially enhance energy values while thermal conductivity rises with increasing temperature and bond length. Conversely, thermal resistivity decreases exponentially with temperature, underscoring the semiconducting behavior of the material.

1. Introduction

Further miniaturization of microelectronic components like transistors into computer chips may become impossible in the near future due to the fundamental laws of physics that govern the principle of operations of transistors manufactured or fabricated from silicon, which may elicit some technical problems in the areas of power consumption, heat, and current leakage. Consequently, there is a need to search for new materials whose properties or features are well suited to address these problems envisaged by the current silicon-based technology [1, 2]. One material seen as a potential replacement for silicon-based transistors is carbon nanotubes (CNTs). CNTs are one of the strongest materials with high elasticity and high conductivity. They are miniature in size and have good stability, and their robust nature allows them to withstand chemically hostile environments. This miniature nature and their high surface area make them suitable candidates for the attachment and assembly of nanoparticles (NPs) on their surface. Their electrical, magnetic, and physical properties can be improved significantly when their internal cavity or external surface is decorated with different inorganic NPs using various experimental procedures [3, 4].

Carbon nanotubes are graphene sheets rolled around a central axis, forming hollow cylindrical shapes. CNTs are of two types-single-walled carbon nanotubes (SWCNT) and multi-walled carbon nanotubes (MWCNT) [5]. Due to the small nanoscale diameter, the confinement and movement of electrons are along their length; hence, CNTs are regarded as 1D nanomaterials [6]. The SWCNTs are rolled-up cylindrical sheets of graphene made up of a benzene type hexagonal network of carbon atoms that are sp^2 hybridized. Their diameters range from 1 to 2 nanometers with lengths of several micrometers to centimeters. MWCNTs comprise layers of graphene sheets rolled up to form a concentric tubular shape. They can be regarded as arrays of concentric SWCNTs stacked in between each other with a spacing of about 0.34 nanometers [7, 8].

Single-walled carbon nanotubes can be metallic or semiconducting in behavior based on their stacking or arrangement of the carbon atoms or their structural features and chirality [9, 10]. Various authors have given similar reasons or more on the metallic or semiconducting nature of CNTs in determining the electronic properties of carbon nanotubes. For instance, how the graphene sheet is rolled up to form determines single-walled carbon nanotubes' metallic or semiconducting behavior. From the aspect of the diameter, a nanotube of a particular diameter is categorized into metallic, small band-gap semiconductor, and moderate band-gap semiconductor, respectively [11]. Carbon nanotubes' metallic or semiconducting nature has been attributed to the diameter and helicity of the carbon atoms in the nanotube's shells [12]. In their experimental work, four probe measurements were done on single nanotubes prepared by different methods. A comparison of various samples was done from the samples of two-probe measurements. They measured

the various samples in terms of the electrical conductivities and resistivities with respect to temperature. From their findings, single nanotubes with a diameter of the likelihood of thirty nanometers (30nm) could exhibit metallic or semiconducting behavior based on helicity. They suggested that the semiconducting nanotubes should have up to thirty nanometers (30nm) diameters. However, the geometrical differences and structural defects were not ruled out in the electrical or electronic properties of the carbon nanotubes [12]. The electronic properties of CNTs have been reported to be highly influenced by geometric differences like defects, chirality, different diameters, etc [13]. Skâkalova *et al.* mentioned that the type of the single-walled carbon nanotubes coupled with the experimental configuration and condition of emergence determine the electronic transport properties of single-walled carbon nanotubes individually [14]. In establishing both the metallic and the semiconducting features of single-walled carbon nanotubes (SWCNTs), Dass *et al.* studied analytically the chirality dependence of electronic band structure and density of states. Their results were compared with simulated values, and SWCNTs' metallic and semiconducting nature was affirmed. From their reports, all armchair SWCNTs showed metallic behavior, while zig-zag SWCNTs exhibited both metallic and semiconducting features [15]. The Aharonov-Bohm (AB) phase created around a cylindrical nanotube in a magnetic field parallel to its axis alters the band structure. A metallic CNT can be transformed into a semiconducting CNT, and a semiconducting tube can become metallic due to the effect of the applied magnetic field. This situation results in unusual behavior of magnetoresistance [3, 16]. Also, a magnetic field's presence can alter carbon nanotubes' electrical properties. For instance, when placed inside a magnetic field, semiconducting carbon nanotubes could be transformed into metallic CNTs. The presence of a magnetic field causes the band gap of semiconducting nanotubes to shrink [17]. Michael reported how the magnetic field affects the metallicity of CNTs. According to them, metallic CNTs can become semiconductors CNTs by applying a minute external magnetic field parallel to the tubes. Semiconducting CNTs can be made metallic under an ultra-high magnetic field [18].

CNTs are very good thermal conductors and can withstand high temperatures. The strong carbon-carbon chemical bonding accounts for their high thermal conductivity. Compared to copper wire, CNTs can transmit over 15 times the amount of energy [19, 1]. The thermal conductivity of aligned bundles of SWNTs is reported to be greater than $200W/mk$ at room temperature. The thermal conductivity of CNTs gives us helpful insight into the low-energy phonon structure of nanotubes [3]. Thermal conductivity (k) of a substance or material is a consequence of the transportation of energy through electrons or lattice vibrations (phonons) [20]. This high thermal conductivity is being utilized in designing and developing heat removal devices that are CNTs-based to help dissipate heat generated by integrated circuits (ICs) [3]. CNTs can exhibit a temperature-dependent resistivity when under the influence of thermal energy. This phenomenon is referred to as the thermo resistivity of CNT. Thermo resistivity refers to the electrical resistance response of a material to changes in temperature difference. Single-walled carbon nanotubes that are semiconducting in nature have negative thermo resistivity. So, the electrical resistivity decreases with an increase in temperature. Metallic single-walled carbon nanotubes have positive thermo resistivity, and electrical resistivity increases with temperature increases [10].

In a bid to search for a material whose device applications can be miniaturized and as well perform optimally, we intend to study analytically with Deng-Fan-Hulthen potential the thermal conductivity and resistivity properties of zig-zag single-walled (8, 0) carbon nanotube in the presence of magnetic and Aharonov-Bohm (AB) flux fields. Zig-zag single-walled (8, 0) carbon nanotube has a length of 6.403(Å) and symmetry group, P4/mmm [21]. The density of the state at the Fermi energy is zero, which depicts its semiconducting nature. It has a calculated band gap of 1.360eV and a simulated band gap of 1.4078eV, respectively. The total number of unit cells and carbon atoms in the overall unit cells is 16 and 32, respectively. The total number of unit cells, carbon atoms, and hexagons in its molecular structure is 208, 416, and 192 [15, 22].

The Deng-Fan-Hulthen potential consists of two different potentials, Deng-Fan and Hulthen potentials, which can be used to study molecular systems. The radial part of the Schrödinger wave equation will be solved analytically with the Nikiforov-Uvarov (NU) method to obtain the energy equation and the wave function. The partition function will be calculated to enable us to determine the thermal conductivity and resistivity of a zig-zag single-walled (8, 0) carbon nanotube.

The organization of this paper is as follows: in section 2, the quantum Hamiltonian of a charged particle placed in our potential under the combined influence of an external magnetic field B and Ahanorov-Bohm (AB) flux, where the Schrödinger wave equation is solved analytically, is considered. The partition function used to evaluate the thermodynamic properties of conductivity and resistivity is calculated in section 3. Our results and discussion are done in section 4. The conclusion is done in the last section followed by the references.

2. Theoretical Model and Formulation

In the cylindrical coordinate system, we write the quantum Hamiltonian of a charged particle kept in a region Deng-Fan-Hulthen potential) under the combined influence of an external magnetic field B and Ahanorov-Bohm (AB) flux as:

$$\frac{1}{2\mu}(i\hbar\vec{\nabla}-\frac{q}{c}\vec{A})^2+D_e\left(1-\frac{\eta}{(e^{\lambda r}-1)}\right)^2-\frac{V_o e^{\lambda r}}{(1-e^{-\lambda r})}=E_{(n,m)}\psi_{(\rho,\varphi,z)} \quad (1)$$

where $\eta = e^{\lambda r_e}$ -1, D_e represents the dissociation energy, r_e stands for the molecular bond length, r is the internuclear distance, λ, is the range of the potential well and V_o stands for the potential strength [23].

Here, μ, is taken to be the effective mass for single-walled carbon nanotubes. The vector potential $\vec{A}$ is written as the summation of two terms, $\vec{A}=\vec{A}_1+\vec{A}_2$ and $\nabla\times\vec{A}_1=\vec{B}$ and $\nabla\times\vec{A}_2=0$ is the symmetric or Coulomb gauge. B_z is the applied magnetic field along the z-direction. The additional magnetic flux Φ_{AB} is due to a solenoid. So, in the cylindrical coordinate system, the vector potential has the azimuthal components written as [24]:

$$\vec{A}_1=\frac{\vec{B}e^{-\vartheta r}}{(1-e^{-\vartheta r})},\quad \vec{A}_2=\frac{\Phi_{AB}}{2\pi r}\hat{\Phi}\ .\ \text{So,}\quad \vec{A}=\left(0,\frac{\vec{B}e^{-\vartheta r}}{(1-e^{-\vartheta r})}+\frac{\Phi_{AB}}{2\pi r},0\right) \quad (2)$$

The Deng-Fan-Hulthen Potential, which is our confining potential, combines two different potentials: Deng-Fan and Hulthen. Below is the graphical behavior of the potential model.

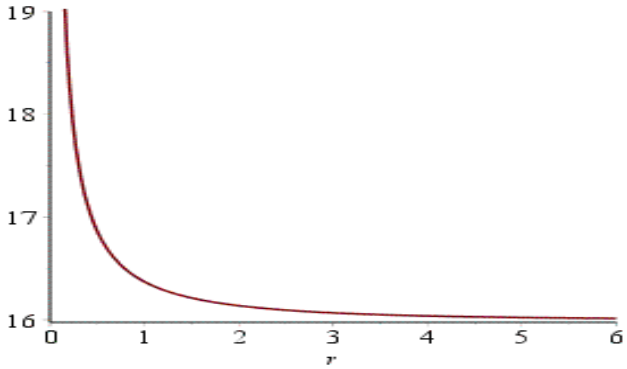

Fig 1 Deng-Fan-Hulthen Potential graphical behaviour

In the cylindrical coordinates, our wave function is taken as:

$$\psi_{(r,\varphi)}=\frac{1}{\sqrt{2\pi}}e^{im\varphi}\ U_{nm,}(r)\ m=0,\pm1,\pm2\ldots \quad (3)$$

where m represents the magnetic quantum number. By inserting our potential, vector potential, and the wave function into Eq. (1), a second-order differential equation of the form will be obtained:

$$\frac{d^2U_{nm}(r)}{dr^2}+\frac{2\mu}{\hbar^2}[E-D_e(1-\frac{\eta}{(e^{\lambda r}-1)})^2+\frac{V_o e^{-\lambda r}}{(1-e^{-\lambda r})}-\frac{2\hbar me\lambda\vec{B}e^{-\lambda r}}{c(1-e^{-\lambda r})}-\frac{e^2\vec{B}e^{-2\lambda r}}{c^2(1-e^{-\lambda r})^2}-\frac{e^2\vec{B}\Phi_{AB}e^{-\lambda r}}{c^2(1-e^{-\lambda r})^2 2\pi r}-\frac{((m+\zeta)-\frac{1}{4})}{r^2}]U_{nm}(r)=0$$
(4)

Since this differential equation contains both exponential and radial terms, an improved approximation scheme by Greene and Aldrich, given in the equation below, will help to solve the equation [23].

$$\frac{1}{r^2}\approx\lambda^2[d_o+\frac{e^{-\lambda r}}{(1-e^{-\lambda r})^2}] \quad (5)$$

By inserting Eq. (5) into Eq. (4) we have

$$\frac{d^2U_{nm}(r)}{dr^2}+[\frac{2\mu E}{\hbar^2}-\frac{2\mu D_e}{\hbar^2}+\frac{4\mu D_e\eta e^{-\lambda r}}{\hbar^2(1-e^{-\lambda r})}\frac{2D_e\eta^2e^{-2\lambda r}}{\hbar^2(1-e^{-\lambda r})^2}+\frac{2V_o e^{-\lambda r}}{\hbar^2(1-e^{-\lambda r})}-\frac{2m\eta\lambda\vec{B}e^{-\lambda r}}{\hbar^2(1-e^{-\lambda r})^2}-\frac{\eta^2\overrightarrow{B^2}e^{-2\lambda r}}{\hbar^2(1-e^{-\lambda r})^2}-\frac{\eta^2\lambda\vec{B}\Phi_{AB}e^{-\lambda r}}{\hbar^2(1-e^{-\lambda r})^2\pi}-((m+\zeta)-\frac{1}{4})\lambda^2(d_o+\frac{e^{-\lambda r}}{(1-e^{-\lambda r})^2})]U_{nm}(r)=0 \quad (6)$$

Where $\eta=\frac{e}{c}$, $\Phi_o=\frac{\hbar c}{e}$, $\zeta=\frac{\Phi_{AB}}{\Phi_o}$ and $\eta=e^{\vartheta r}-1$, c is the speed of light.

Using the transformation $z=e^{-\lambda r}$ (7)

After differentiating twice, you will obtain:

$$\frac{d^2}{dz^2} = \frac{\lambda^2 z^2 d^2}{dz^2} + \frac{\lambda^2 z d}{dz} \quad (8)$$

Substituting Eq. (8) into Eq. (6) and divide through by $\lambda^2 z^2$ the result will be:

$$\frac{d^2U_{nm}}{dz^2} + \frac{1}{z}\frac{dU_{nm}}{dz} + \frac{1}{z^2}\left[\frac{2\mu E}{\hbar^2\lambda^2} - \frac{2\mu D_e}{\hbar^2\lambda^2} + \frac{4\mu D_e \eta z}{\hbar^2\lambda^2(1-z)} - \frac{2\mu D_e \eta^2 z^2}{\hbar^2\lambda^2(1-z)^2} + \frac{2\mu V_o z}{\hbar^2\lambda^2(1-z)} - \frac{2m\eta\vec{B}z}{\hbar\lambda(1-z)^2} - \frac{\eta^2\vec{B}^2 z^2}{\hbar^2\lambda(1-z)^2} - \frac{\eta^2\vec{B}\Phi_{AB}z}{\hbar^2\lambda(1-z)^2\pi} - \left((m+\zeta)^2 - \frac{1}{4}\right)\left(d_o + \frac{z}{(1-z)^2}\right)\right] U_{nm}(r) = 0 \quad (9)$$

We use the following dimensionless symbols for mathematical convenience

$$-\varepsilon = \frac{2\mu(E_{nm}-D_e)}{\hbar^2\lambda^2}\ ,\quad \gamma_1 = \frac{4\mu D_e\eta}{\hbar^2\lambda^2}\ ,\quad \gamma_2 = \frac{2\mu D_e\eta^2}{\hbar^2\lambda^2}\ ,\quad d_o = \frac{2\mu V_o}{\hbar^2\lambda^2}\ ,\ \chi = \frac{2m\eta\vec{B}}{\hbar\lambda}, \lambda_1 = \frac{\eta^2\vec{B}^2}{\hbar^2\lambda^2}, \lambda_2 = \frac{\eta^2\vec{B}\Phi_{AB}}{\hbar^2\lambda^2\pi}, V = \left((m+\zeta)^2 - \frac{1}{4}\right) \quad (10)$$

Equation (9) can be rewritten with respect to these dimensionless symbols as:

$$\frac{d^2U_{nm}}{dz^2} + \frac{(1-z)}{z(1-z)}\frac{dU_{nm}}{dz} + \frac{1}{z^2(1-z)^2}[-\varepsilon(1-z)^2 + \gamma_1(1-z)z - \gamma_2(z^2) + d_o(1-z)z - \chi(z) - \lambda_1(z^2) - \lambda_2(1-z)z - Vd_o(1-z)^2 - V(z)]\, U_{nm} = 0 \quad (11)$$

Subsequently, Eq. (11) can be evaluated further as:

$$\frac{d^2U_{nm}}{dz^2} + \frac{(1-z)}{z(1-z)}\frac{dU_{nm}}{dz} + \frac{1}{z^2(1-z)^2}[-(\varepsilon + \gamma_1 + \gamma_2 + d_o + \lambda_1 - \lambda_2 + Vd_o)z^2 + (2\varepsilon + \gamma_1 + d_o - \chi - \lambda_2 + 2Vd_o - V)z - (\varepsilon + Vd_o)]\, U_{nm} = 0 \quad (12)$$

Equation (12) is compared with the parametric form of the NU of Eq. (13) is written as [25]

$$R''_{(z)} + \frac{\tau_1 - \tau_2 z}{z(1-\tau_3 z)}R'_{(z)} + \left[\frac{-\xi_1 z^2 + \xi_2 z - \xi_3}{z^2(1-\tau_3 z)^2}\right]R_{(z)} = 0 \quad (13)$$

The energy eigenvalues equation, according to the NU, is written as

$$\tau_2 n - (2n+1)\tau_5 + (2n+1)\left[\sqrt{\tau_9} + \tau_3\sqrt{\tau_8}\right] + n(n-1)\tau_3 + \tau_7 + 2\tau_3\tau_8 + 2\sqrt{\tau_8\tau_9} = 0 \quad (14)$$

The corresponding wave function is given as:

$$U_{nm}(z) = z^{\tau_{12}}(1 - \tau_3 z)^{-\tau_{12} - \tau_{13}/\tau_3}\, p_n^{\tau_{10}-1,\left(\frac{\tau_{11}}{\tau_3}\right)-(\tau_{10}-1)}(1 - 2\tau_3 z) \quad (15)$$

where the following parameters are written as

$$\tau_4 = \frac{1}{2}(1 - \tau_1) \quad (16)$$

$$\tau_5 = \frac{1}{2}(\tau_2 - 2\tau_3) \quad (17)$$

$$\tau_6 = \tau_5 + \xi_1 \quad (18)$$

$$\tau_7 = 2\tau_4\tau_5 - \xi_2 \quad (19)$$

$$\tau_8 = \tau^2{}_4 + \xi_3 \quad (20)$$

$$\tau_9 = \tau_3\tau_7 + \tau^2{}_3\tau_8 + \tau_6 \quad (21)$$

$$\tau_{10} = \tau_1 + 2\tau_4 + 2\sqrt{\tau_8} \quad (22)$$

$$\tau_{11} = \tau_2 - 2\tau_5 + 2(\sqrt{\tau_9} + \tau_3\sqrt{\tau_8}) \quad (23)$$

$$\tau_{12} = \tau_4 + \sqrt{\tau_8} \quad (24)$$

$$\tau_{13} = \tau_5 - (\sqrt{\tau_9} + \tau_3\sqrt{\tau_8}) \quad (25)$$

When Eq. (12) is compared with the parametric form of the NU of Eq. (13), the following parameters can be found:

$$\tau_1 = \tau_2 = \tau_3 = 1 \quad (26)$$

$$\xi_1 = \varepsilon + \gamma_1 + \gamma_2 + d_o + \lambda_1 - \lambda_2 + Vd_o \quad (27)$$

$$\xi_2 = 2\varepsilon + \mathfrak{y}_1 + \mathfrak{d}_e - \chi - \lambda_2 + 2Vd_o - V \quad (28)$$

$$\xi_3 = \varepsilon + Vd_o \quad (29)$$

From Eqs. (16-21) we obtain

$$\mathfrak{r}_4 = \frac{1}{2}(1 - \mathfrak{r}_1) = 0,\ \mathfrak{r}_5 = \frac{1}{2}(\mathfrak{r}_2 - 2\mathfrak{r}_3) = -\frac{1}{2},\ \mathfrak{r}_6 = \mathfrak{r}_5^2 + \xi_1 = \frac{1}{4} + \varepsilon + \mathfrak{y}_1 + \mathfrak{y}_2 + \mathfrak{d}_e + \lambda_1 - \lambda_2 + Vd_o \quad (30)$$

$$\mathfrak{r}_7 = 2\mathfrak{r}_4\mathfrak{r}_5 - \xi_2 = -(2\varepsilon + \mathfrak{r}_1 + \mathfrak{d}_e - \chi - \lambda_2 + 2Vd_o - V) \quad (31)$$

$$\mathfrak{r}_8 = \mathfrak{r}_4^2 + \xi_3 = \varepsilon + Vd_o \quad (32)$$

$$\mathfrak{r}_9 = \mathfrak{r}_3\mathfrak{r}_7 + \mathfrak{r}_3^2\mathfrak{r}_8 + \mathfrak{r}_6 = \frac{1}{4} + \chi + V + \lambda_1 + \mathfrak{y}_2 \quad (33)$$

Recall that in Eq. (10), $-\varepsilon = \frac{2\mu(E_{nm} - D_e)}{\hbar^2\lambda^2}$ (34)

So, substituting Eqs. (30-33) into Eq. (14) and carrying out some algebra, the energy eigenvalue equation of the Deng-Fan-Hulthen potential is obtained as:

$$E_{nm} = -\frac{\hbar^2\lambda^2}{2\mu}\left[\left(\frac{(\sigma - \Lambda)}{2(\tau + \sqrt{\sigma})} - \frac{(\tau + \sqrt{\sigma})}{2}\right)^2 - Vd_o + D_e\right] \quad (35)$$

Where

$$\sigma = \frac{1}{4} + \chi + V + \lambda_1 + \mathfrak{y}_2,\ \Lambda = -\mathfrak{y}_1 - \mathfrak{d}_e + \chi + \lambda_2 + V, \tau = n + \frac{1}{2} \quad (36)$$

Thus, Eq. (36) can be re-written in terms of the dimensionless symbols of Eq. (10) as:

$$\sigma = \frac{1}{4} + \frac{2m\eta\vec{B}}{\hbar\lambda} + (m + \zeta)^2 - \frac{1}{4} + \frac{\eta^2\vec{B}^2}{\hbar^2\lambda^2} + \frac{2\mu D_e\mathfrak{y}^2}{\hbar^2\lambda^2} \quad (37)$$

$$\Lambda = -\frac{4\mu D_e\mathfrak{y}}{\hbar^2\lambda^2} - \frac{2\mu V_o}{\hbar^2\lambda^2} + \frac{2m\eta\vec{B}}{\hbar\lambda} + \frac{\eta^2\vec{B}\Phi_{AB}}{\hbar^2\lambda\pi} + (m + \zeta)^2 - \frac{1}{4} \quad (38)$$

From Eqs. (22-25) we determine

$$\mathfrak{r}_{10} = \mathfrak{r}_1 + 2\mathfrak{r}_4 + 2\sqrt{\mathfrak{r}_8} = 1 + 2\sqrt{\varepsilon + Vd_0} \quad (39)$$

$$\mathfrak{r}_{11} = \mathfrak{r}_2 - 2\mathfrak{r}_5 + 2(\sqrt{\mathfrak{r}_9 + \mathfrak{r}_3\mathfrak{r}_8} = 2 + 2\left(\sqrt{\frac{1}{4} + \chi + V + \lambda_1 + \mathfrak{y}_2 + \varepsilon + Vd_0}\right) \quad (40)$$

$$\mathfrak{r}_{12} = \mathfrak{r}_4 + \sqrt{\mathfrak{r}_8} = \sqrt{\varepsilon + Vd_0} \quad (41)$$

$$\mathfrak{r}_{13} = \mathfrak{r}_5 - (\sqrt{\mathfrak{r}_9} + \mathfrak{r}_3\sqrt{\mathfrak{r}_8}) = -\frac{1}{2} - \left(\sqrt{\frac{1}{4} + \chi + V + \lambda_1 + \mathfrak{y}_2} + \sqrt{\varepsilon + Vd_0}\right) \quad (42)$$

Substituting Eqs. (39-42) into Eq. (15), the wave function written in Eq. (43) is obtained.

$$U_{nm}(\mathfrak{z}) = \mathfrak{z}^{\sqrt{\varepsilon + Vd_0}}(1 - \mathfrak{z})^{\frac{1}{2} + \sqrt{\frac{1}{4} + \chi + V + \lambda_1 + \mathfrak{y}_2}} P_n^{2\sqrt{\varepsilon + Vd_0},\, 2\sqrt{\frac{1}{4} + \chi + V + \lambda_1 + \mathfrak{y}_2}}(1 - 2\mathfrak{z}) \quad (43)$$

3. The Partition Function and the Thermodynamic Properties of Carbon Nanotube

Thermal conductivity and resistivity are two aspects of the thermodynamic properties of nanotubes that can be determined. To calculate these two properties, the partition function, which is temperature dependent, is first evaluated. The partition function can be evaluated when a direct summation is done over all possible energy levels at a given temperature. The partition function is written as [26]:

$$Z(\beta) = \sum_n^{v_{max}} e^{-\beta E_{n,m}} \quad (44)$$

where $\beta = \frac{1}{KT}$ with K as the Boltzmann constant, T, the temperature E_{nm} is the energy of the nth bound state where $n = 0, 1, 2, 3 \ldots, v_{max}$.

The energy eigenvalue of equation (35) can be re-written as:

$$E_{nm} = -\hbar^2\lambda^2\left(\frac{N_1-(n+\sigma)^2}{2(n+\sigma)}\right)^2 + N_2 \quad (45)$$

Where

$$N_1 = \frac{1}{4} + \frac{2m\eta\vec{B}}{\hbar\lambda} + (m+\zeta)^2 - \frac{1}{4} + \frac{\eta^2\vec{B}^2}{\hbar^2\lambda^2} + \frac{2\mu D_e\eta^2}{\hbar^2\lambda^2} + \frac{4\mu D_e\eta}{\hbar^2\lambda^2} - \frac{2\mu V_o}{\hbar^2\lambda^2} + \frac{2m\eta\vec{B}}{\hbar\lambda} + \frac{\eta^2\vec{B}\Phi_{AB}}{\hbar^2\lambda\pi} + (m+\zeta)^2 - \frac{1}{4} \quad (46)$$

$$N_2 = \left((m+\zeta)^2 - \frac{1}{4}\right) d_o\left(\frac{\hbar^2\lambda^2}{2\mu}\right) + D_e \quad (47)$$

Therefore, equation (44) can be recast as:

$$Z(\beta) = \sum_n^{v_{max}} e^{-\beta\left[-\frac{\hbar^2\lambda^2}{2\mu}\left(\frac{N_1-(n+\sigma)^2}{2(n+\sigma)}\right)^2 + N_2\right]} \quad (48)$$

In the classical limit, the summation of equation (48) is replaced by an integral therefore, we have

$$Z_{(\beta)} = \int_0^v e^{\left(Pl^2\beta + \frac{G\beta}{l^2} + M\beta\right)} dl, l = n+\sigma \quad (49)$$

Where

$$P = \frac{\hbar^2\lambda^2}{8\mu}, G = -\frac{\hbar^2\lambda^2 N_1^2}{8\mu}, M = -\left(\frac{\hbar^2\lambda^2 N_1}{4\mu} + N_2\right) \quad (50)$$

The Maple software is used to evaluate equation (49) to obtain the partition function of the system as:

$$\frac{1}{2} e^{P.\beta.l^2 + M.\beta\sqrt{G.\beta}} \left(\frac{2.v.e^{\frac{G.\beta}{v^2}}}{\sqrt{G.\beta}} - \frac{2\sqrt{G.\beta}\ \sqrt{\pi}\ erfi\left(\frac{G.\beta}{v}\right)}{\sqrt{G.\beta}} - 2\sqrt{\pi}\right) \quad (51)$$

Where $erfi$ (k) denotes the imaginary error function [27] defined as

$$\text{erfi}(k) = ierf(k) = \frac{2}{\sqrt{\pi}}\int_0^k e^{t^2} dt \quad (52)$$

In Maple software, this error function is used for various numerical calculations.

With the partition function of the system known, the thermal conductivity K, which is a function of heat capacity, phonon group velocity and the free mean path can be. The thermal conductivity of CNTs can be written as [28]:

$$K = \frac{1}{3}\rho c v^2 \tau_s \quad (53)$$

Here, c, v, and τ stand for specific heat per unit volume, group velocity, and relaxation time or free mean path of a given phonon state, respectively [29]. The specific heat capacity is given by the relation [30]:

$$\text{Specific heat } C_v = \frac{\partial U}{\partial T} = k_B\beta^2\frac{\partial^2 lnZ}{\partial\beta^2} \quad (54)$$

So we can write the thermal conductivity as:

$$\text{Thermal conductivity } K = \frac{1}{3}\rho v^2\tau_s k_B\beta^2\frac{\partial^2 lnZ}{\partial\beta^2} \quad (55)$$

Thermal resistivity is obtained from the reciprocal thermal conductivity of Eq. (55).

4. Results and Discussion

In Figures 2 and 3, we present graphical plots of energy variation with magnetic field and Aharonov-Bohm (AB) flux, respectively.

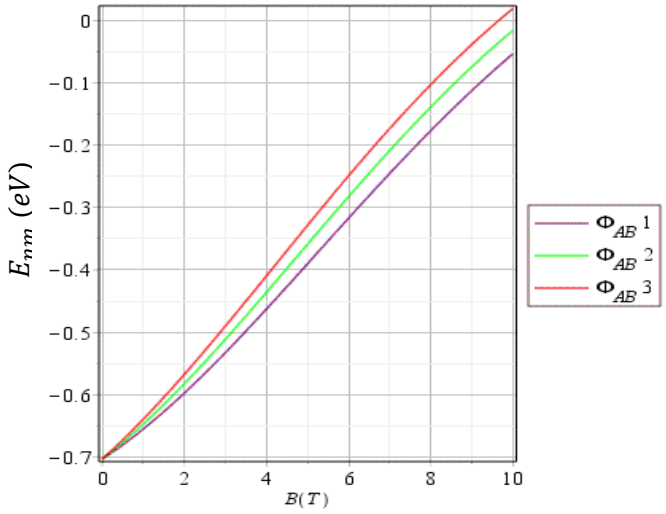

Fig. 2: Plot of Energy, E versus magnetic field B

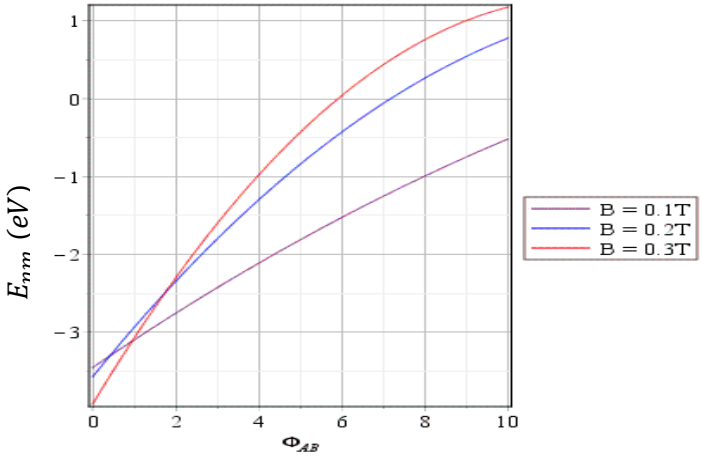

Fig. 3: Plot of Energy, E versus AB flux

Figures 4 and 5 show graphical plots of the thermal conductivity with temperature variation and bond length.

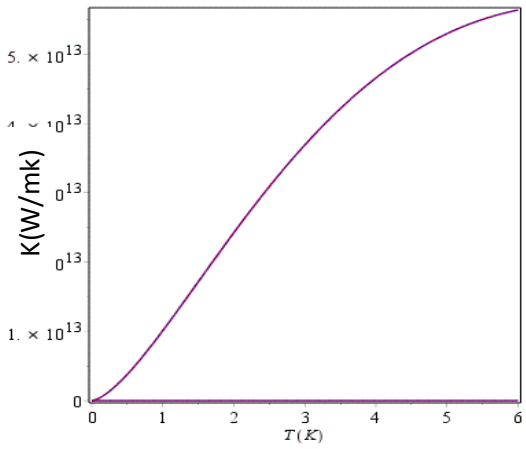

Fig. 4: Plot of thermal conductivity versus temperature

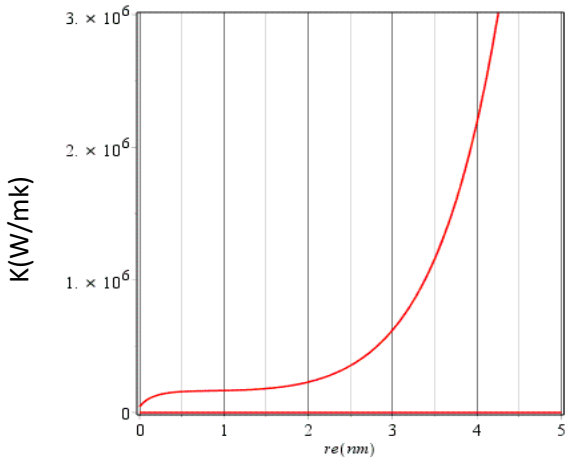

Fig. 5 Plot of thermal conductivity versus bond length

Here is the graphical plot of thermal resistivity versus temperature

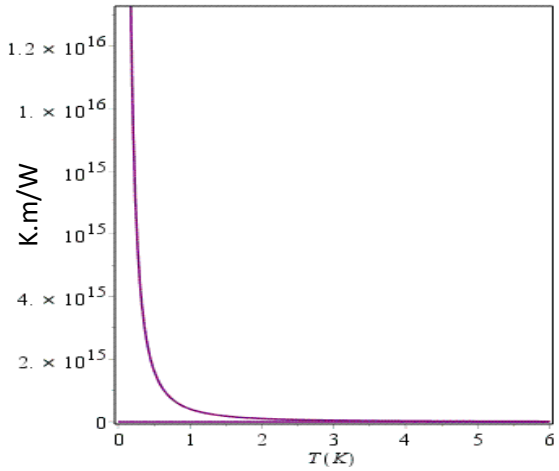

Fig. 6: Plot of thermal resistivity versus temperature

Figure 2 shows the plot of the energy, E with the varying magnetic field $\vec{B}$ at different values of the AB flux. It can be seen that the energy values show an exponential rise as the magnetic field strength increases. Figure 3 depicts the plot of the energy E against Aharonov-Bohm (AB) flux Φ_{AB} for the respective values of$0.1T$, $0.2T$ and $0.3T$ of the magnetic field strength. As the AB flux increases exponentially, the energy values increase correspondingly. So, both fields' notable impacts on increasing energy values can be seen. In Figure 4, the plot of thermal conductivity with temperature variations is shown; from the plot, the thermal conductivity values show an exponential increase with the temperature. The phonon scattering accounts for this behavior. The thermal conductivity versus the bond length is shown in Figure 5. The thermal conductivity increases exponentially as the bond length increases. This phenomenon results from the increase in the thermal transport which varies proportionally with the SWCNT bond length. Also, the phonon wavelength that serves as a medium for thermal transport increases as the bond length increases. Figure 6 shows the plot of thermal resistivity with the temperature. It is seen that the thermal resistivity decreases as the temperature increases. As the concentration of the thermally generated electron-hole pairs increases, the thermal resistivity of our zig-zag single-walled (8,0) decreases with the increasing temperature. The carrier scattering on phonons also accounts for this phenomenon or behavior. This graphical behavior of Figure 6 tells us that zig-zag single-walled (8,0) is semiconducting in nature.

5. Conclusion

The analytical solution of the energy eigenvalue of the Schrödinger wave equation with the Deng-Fan-Hulthen potential was obtained with the Nikiforov-Uvarov method. The effects of the magnetic and Aharonov-Bohm (AB) flux fields on the energy eigenvalue were analyzed graphically. Our results showed that both fields increased exponentially with the energy eigenvalues. The partition function calculated was used to evaluate the thermodynamic properties of conductivity and resistivity in terms of temperature and bond length. The thermal conductivity of our nanotube increased exponentially with the temperature and the bond length, while the thermal resistivity decreased exponentially with temperature. From the graphical plot of Figure 6, zig-zag SWCNT (8, 0) exhibited a semiconducting feature. This agrees with the work of Dass and Vaid [15] cited within. Thus, this semiconducting SWCNT can be a promising material for fabricating high-performing field effect transistors (FETs) in the electronics industry. Also, the good thermal conductivity nature of this nanotube could be utilized in the thermal management system of thermoelectric materials.

Statements and Declaration

Authors Contributions

Ikechukwu Otete: Conceived the concept and designed the analysis; analyzed and interpreted the data. Wrote the paper.

Isaac Chukwutem Abiodun: Analyzed and interpreted the data. Wrote the paper.
Ikenna Emmanuel Odezuligbo: Proofread and edited the paper.

Funding Statement

The authors did not receive any funding from any organization.

Conflict of Interest

The authors declare no conflict of interest.

References

1. Fakhar Anjum. Spintronics: Fundamentals and Applications. EE453 Project Report.; 2008.
2. Novoselov K, Geim A, Morozov S, et al. Electric Field Effect in Atomically Thin Carbon Films. Nat Mater. 2004;6.
3. Jorio A, Dresselhaus G, Dresselhaus M. Carbon Nanotubes: Advanced Topics in the Synthesis, Structure, Properties and Applications. Vol 111.; 2008. doi:10.1007/978-3-540-72865-8
4. Kim IT, Tannenbaum R. Magnetic Carbon Nanotubes: Synthesis, Characterization, and Anisotropic Electrical Properties. In: ; 2011. doi:10.5772/22636
5. Kardan H, Maraki M, Rajaei A. Application of Carbon Nanotubes(CNT) on The Computer Science and Electrical Engineering: A Review. International Journal of Reconfigurable and Embedded Systems (IJRES). 2020;9:61. doi:10.11591/ijres.v9.i1.pp61-82
6. H.-S. Philip Wong and Deji Akinwande. Carbon Nanotube and Graphene Device Physics by. Contemporary Physics - CONTEMP PHYS. 2012;53:1. doi:10.1080/00107514.2012.689336
7. Saifuddin NM, Raziah AZ, Junizah AR. Carbon Nanotubes: A Review on Structure and Their Interaction with Proteins. J Chem. 2013;2013. doi:10.1155/2013/676815
8. Nanot S, Thompson N, Kim JH, et al. Single-Walled Carbon Nanotubes. In: Springer Handbook of Nanomaterials. ; 2013:105-146. doi:10.1007/978-3-642-20595-8_4
9. Avouris P, Appenzeller J, Martel R, Wind SJ. Carbon nanotube electronics. Proceedings of the IEEE. 2003;91:1772-1784. doi:10.1109/JPROC.2003.818338

10. Aviles F. Thermoresistivity of Carbon Nanostructures and their Polymeric Nanocomposites. Adv Mater Interfaces. 2023;10. doi:10.1002/admi.202300218

11. Morkoç H. Advanced Semiconductor and Organic Nano-Techniques.; 2003.

12. Ebbesen T, Lezec H, Hiura H, Bennett J, Ghaemi H, Thio T. Electrical conductivity of individual carbon nanotubes. Nature. 1996;382:54-56. doi:10.1038/382054a0

13. Saeed K. Carbon nanotubes–properties and applications: a review. Carbon letters. 2013;14:131-144. doi:10.5714/CL.2013.14.3.131-

14. Skákalová V, Kaiser A, Woo Y, Roth S. Electronic transport in carbon nanotubes: From individual nanotubes to thin and thick networks. Phys Rev B. 2006;74. doi:10.1103/PhysRevB.74.085403

15. Dass D. Chirality dependence of electronic band structure and density of states in single-walled carbon nanotubes. African Review of Physics. 2018;12.

16. Ovchinnikov AA, Atrazhev V. Magnetic susceptibility of multilayered carbon nanotubes. Physics of the Solid State. 1998;40:1769. doi:10.1134/1.1130653

17. Sanjay Kumar Karna. Properties and Applications of Carbon Nanotubes.; 2007.

18. Michael J. O'Connell. Carbon Nanotubes Properties and Applications.; 2006. doi:https://doi.org/10.1201/9781315222127

19. Khanna S, Islam N. Carbon Nanotubes-Properties and Applications. Organic & Medicinal Chemistry International Journal. 2018;7(1):30-35. doi:10.19080/OMCIJ.2018.07.55

20. Rockett Angus. The Physics of Solids. In: The Materials Science of Semiconductors. Springer US; 2008:21-72. doi:10.1007/978-0-387-68650-9_2

21. Zeinalipour-Yazdi C, Loizidou E, Chutia A. Size-Dependent Bond Dissociation Enthalpies in Single-Walled Carbon Nanotubes. Chem Phys Lett. 2019;731:136628. doi:10.1016/j.cplett.2019.136628

22. Dass D, Prasher R, Vaid R. Analytical Study of Unit Cell and Molecular Structures of Single-Walled Carbon Nanotubes. International Journal of Computational Engineering Research. 2012;2.

23. Ikot A, Okorie U, Amadi P, Edet C, Rampho G, Sever R. The Nikiforov–Uvarov-Functional Analysis (NUFA) Method: A New Approach for Solving Exponential-Type Potentials. Few Body Syst. 2021;62. doi:10.1007/s00601-021-01593-5

24. Ikhdair S, Falaye B, Hamzavi M. Nonrelativistic Molecular Models Under External Magnetic and AB Flux Fields. Ann Phys (N Y). 2015;353:282–298.

25. Otete I, Eleje CB. Magnetic Field Effect on the Energy Spectra of Indium Phosphide (InP) Quantum dot in D-dimensions with the Hulthen-Yukawa Potential. Asian Research Journal of Current Science. 2023;5(1):20-27. https://jofscience.com/index.php/ARJOCS/article/view/31

26. Ikot A, Okorie U, Ngiangia A, et al. Bound state solutions of the Schrödinger equation with energy- dependent molecular Kratzer potential via asymptotic iteration method. Eclética Química. 2020;45:65-76. doi:10.26850/1678-4618eqj.v45.1.2020.p65-77

27. Edet C, Okoi P, Yusuf A, O U, Amadi P. Bound state solutions of the generalized shifted Hulthén potential. Indian Journal of Physics. 2020;95. doi:10.1007/s12648-019-01650-0

28. Wu MCH, Hsu JY. Thermal conductivity of carbon nanotubes with quantum correction via heat capacity. Nanotechnology. 2009;20:145401. doi:10.1088/0957-4484/20/14/145401

29. Tonpheng B. Thermal and Mechanical Studies of Carbon Nanotube-Polymer Composites Synthesized at High Pressure and High Temperature.; 2011.

30. Khordad R, Rastegar H. Thermodynamic Properties of a Double Ring-Shaped Quantum Dot at Low and High Temperatures. J Low Temp Phys. 2018;190:1-13. doi:10.1007/s10909-017-1831-x